Laminar Heat Transfer With Viscous Dissipation and Fluid Axial Heat Conduction for Modified Power Law Fluids Flowing in Parallel Plates With One Plate Moving*

Toru SHIGECHI**, Ganbat DAVAA***
Satoru MOMOKI** and Odgerel JAMBAL***

Using the fully developed laminar velocity distributions obtained by applying the modified power-law model proposed by Irvine and Karni, the thermal-entrance-region heat transfer of non-Newtonian fluids flowing in parallel plates with one plate moving is investigated taking into account both viscous dissipation and fluid axial heat conduction for two kinds of thermal boundary conditions, namely, constant temperature and constant heat flux at the moving wall. The energy equation subject to a constant temperature at upstream infinity, fully developed temperature profile at downstream infinity and the appropriate thermal boundary conditions at the upper and lower walls is numerically solved by the finite difference method as an elliptic type problem. The effects of the moving plate velocity, rheological properties, Brinkman number and Peclet number on the temperature distribution and Nusselt numbers are discussed for both Newtonian and pseudoplastic fluids.

Key Words: Non-Newtonian Fluids, Moving Boundary, Viscous Dissipation, Fluid Axial Heat Conduction, Thermal Entrance Region

1. Introduction

Problems involving fluid flow and heat transfer in an annular or parallel-plate geometry with a moving boundary of solid body or liquid can be found in many manufacturing processes such as extrusion, drawing, polymer coatings of wires (or tubes) for corrosion protection and hot rolling, etc. In such processes, the moving body continuously exchanges heat with the surrounding environment. For such cases, the fluid involved may be Newtonian or non-Newtonian and the flow situations encountered can be either laminar or turbulent.

Many important industrial fluids are non-Newtonian in the flow characteristics. The power-law model is frequently used in non-Newtonian fluid flow and heat transfer analyses to predict the behavior of pseudoplastic or dilatant fluids. However, this power-law model has a drawback that the correct velocity field is not ensured if the power-law model is applied to the region of lower shear rates including zero shear rate. To accommodate the power-law model to lower regions of shear rate, a modified power-law model has been proposed by Irvine and Karni[1].

Viscous dissipation is generated by the velocity gradient of the flowing fluid. The moving wall deforms the velocity profile and the velocity gradient is changed. Therefore, it is important to clarify the effect of viscous dissipation for the parallel-plate geometry with a moving plate using the accurate velocity distributions.

Thermally developing heat transfer of non-Newtonian fluids in parallel plates with one plate moving was investigated by Lin[2]. The thermal boundary conditions adopted by Lin are not the same as those of our study. In his study the power law model was applied and the effect of fluid axial heat conduction was neglected.

In this study, using the fully developed laminar

* Received 28th April, 2003 (No. 03-4046)
** Department of Mechanical Systems Engineering, Nagasaki University, 1-14 Bunkyo-machi, Nagasaki 852-8521, Japan. E-mail: shigechi@net.nagasaki-u.ac.jp
*** Graduate School of Science and Technology, Nagasaki University. E-mail: davaa@celcius.mech.nagasaki-u.ac.jp

velocity field obtained by applying the modified power-law model, the effect of viscous dissipation and fluid axial heat conduction on thermal entrance-region heat transfer of non-Newtonian fluids flowing in parallel plates with one plate moving is investigated for the thermal boundary conditions of constant temperature and constant heat flux at the moving wall. The effects of the moving wall velocity, flow index of the modified power-law fluid, Brinkman number and Peclet number on the temperature distribution and Nusselt number at the walls are discussed.

Nomenclature

Br : Brinkman number
C : coefficient in Eq.(35)
c_p : specific heat at constant pressure
D_h : hydraulic diameter $=2L$
f : friction factor
h : heat transfer coefficient
k : thermal conductivity
L : distance between parallel plates
m : fluid consistency
n : flow index
Nu : Nusselt number
P : pressure
Pe : Peclet number
q : heat flux
Re_M : modified Reynolds number $=\frac{\rho u_m D_h}{\eta}$
Pr_M : modified Prandtl number $=\frac{c_p \eta}{k}$
T : temperature
u : fully developed velocity profile
u_m : average velocity of the fluid
u^* : dimensionless velocity $=u/u_m$
U : axial velocity of the moving plate
U^* : dimensionless relative velocity of the moving plate $=U/u_m$
y : coordinate normal to the fixed plate
y^* : dimensionless coordinate $=y/D_h$
z : axial coordinate
z^* : dimensionless axial coordinate $=z/(PeD_h)$
β : dimensionless shear rate parameter
η_a : apparent viscosity
η_a^* : dimensionless apparent viscosity $=\eta_a/\eta$
η_0 : viscosity at zero shear rate
η : reference viscosity
ρ : density
τ : shear stress
θ : dimensionless temperature

Subscripts

b : bulk
e : inlet
fd : fully developed
j : I for Case I or II for Case II
lw : lower wall
uw : upper wall

2. Analysis

We consider thermally developing and hydrodynamically developed laminar flow of non-Newtonian fluids between parallel plates subjected to constant wall temperature (Case I) and constant wall heat flux (Case II). The physical model for the analysis is shown in Fig. 1. The lower plate moves axially at a constant velocity, U. The assumptions used in the analysis are:

- The flow is incompressible, steady-laminar, and fully developed hydrodynamically.
- The fluid is non-Newtonian and the shear stress may be described by the modified power-law model[1], and physical properties are constant.

2.1 Fluid flow

With the assumptions described above, the governing momentum equation is

$$\frac{d\tau}{dy}=-\frac{dP}{dz}. \tag{1}$$

The boundary conditions are:

$$\text{B.C.}: \begin{cases} u=0 & \text{at} \quad y=0 \\ u=U & \text{at} \quad y=L. \end{cases} \tag{2}$$

The shear stress, τ, in Eq.(1) is given by the modified power law model[1].

$$\tau=-\eta_a\frac{du}{dy} \tag{3}$$

where η_a is the apparent viscosity for pseudoplastic fluids ($n<1$), defined by

$$\eta_a=\frac{\eta_0}{1+\frac{\eta_0}{m}\left|\frac{du}{dy}\right|^{1-n}}. \tag{4}$$

The average velocity, u_m, is defined as

$$u_m\equiv\frac{1}{L}\int_0^L u\,dy. \tag{5}$$

The momentum equation and its boundary conditions are reduced to, in dimensionless form, as

$$\frac{d}{dy^*}\left(\eta_a^*\frac{du^*}{dy^*}\right)=-2f\cdot Re_M \tag{6}$$

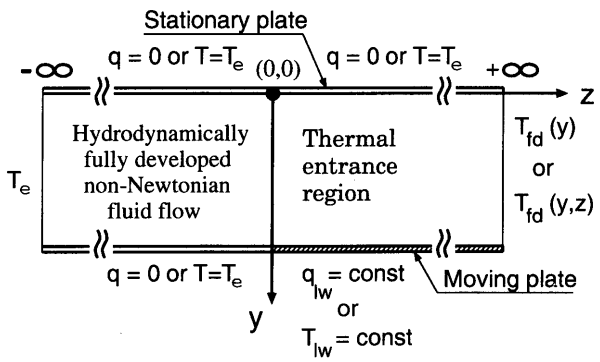

Fig. 1 Physical model

$$\text{B.C.}: \begin{cases} u^*=0 & \text{at} \quad y^*=0 \\ u^*=U^* & \text{at} \quad y^*=1/2 \end{cases} \tag{7}$$

where

$$y^*=\frac{y}{D_h}, \quad u^*=\frac{u}{u_m}. \tag{8}$$

Friction factor, f, and modified Reynolds number, Re_M, are defined as

$$f\equiv\frac{D_h}{2\rho u_m^2}\left(-\frac{dP}{dz}\right), \quad Re_M\equiv\frac{\rho u_m D_h}{\eta}. \tag{9}$$

The dimensionless apparent viscosity, η_a^*, is defined as

$$\eta_a^*\equiv\frac{\eta_a}{\eta}=\frac{1+\beta}{1+\beta\left|\frac{du^*}{dy^*}\right|^{1-n}} \quad \text{for} \quad n<1. \tag{10}$$

From Eq.(10) developed for the modified power law fluids, the following expressions are obtained at the asymptotes of $\beta\to 0$ and $\beta\to\infty$, respectively. The former stands for a Newtonian fluid and the latter for a power law fluid.

$$\eta_a^*\Rightarrow 1 \quad \text{for} \quad \beta\to 0$$

$$\eta_a^*\Rightarrow\left|\frac{du^*}{dy^*}\right|^{n-1} \quad \text{for} \quad \beta\to\infty$$

where

$$\eta=\frac{\eta_0}{1+\beta} \qquad \beta=\frac{\eta_0}{m}\left(\frac{u_m}{D_h}\right)^{1-n}. \tag{11}$$

β is a parameter, which represents the effects of the average velocity, u_m, and the hydraulic diameter, D_h, when the rheological parameters of a non-Newtonian fluid; η_0, n and m, are prescribed. β increases with an increase in u_m or a decrease in D_h for $n<1$.

The dimensionless form of Eq.(5) is

$$1=2\int_0^{1/2} u^* dy^*. \tag{12}$$

The dimensionless velocity, u^*, is numerically determined from Eqs.(6), (7) and (12). First, we assume the value of $f\cdot Re_M$ for a given set of parameters: n, β and U^* to solve Eq.(6) together with Eq.(7). Then, Eq.(12) is checked by substituting the resulting velocity distribution, u^*, into it. Unless Eq.(12) is satisfied within the accuracy of 10^{-5}, the value of $f\cdot Re_M$ is updated. This process is repeated until the correct value of $f\cdot Re_M$ is obtained.

The detailed analysis and results are given in Ref.(3). The typical velocity profile and its square of velocity gradient is shown in Fig. 2 for a pseudoplastic fluid ($n=0.5$ and $\beta=1$) corresponding to $U^*=0$ and 1.

2.2 Heat transfer

The energy equation together with the assumptions above is written as

$$\rho c_p u\frac{\partial T}{\partial z}=k\left(\frac{\partial^2 T}{\partial y^2}+\frac{\partial^2 T}{\partial z^2}\right)+\eta_a\left(\frac{du}{dy}\right)^2 \tag{13}$$

$$\text{in} \quad 0<y<L \quad \text{and} \quad -\infty<z<\infty$$

Case I: constant wall temperature

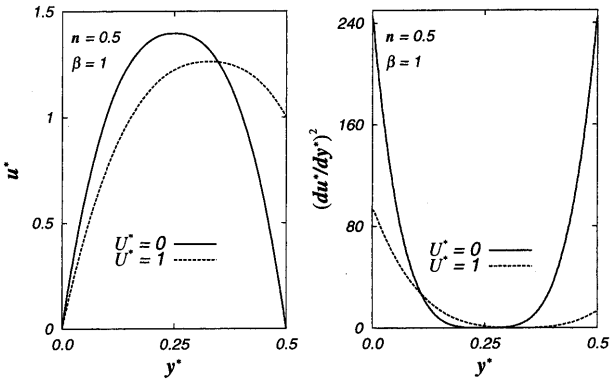

Fig. 2 Velocity profile and square of velocity gradient ($n=0.5$, $\beta=1$)

$$\begin{cases} T=T_e & \text{at} \quad y=0 & \text{for} \quad 0<z \\ T=T_{\text{lw}} & \text{at} \quad y=L & \text{for} \quad 0<z \\ T=T_e & \text{at} \quad y=0 & \text{for} \quad z\le 0 \\ T=T_e & \text{at} \quad y=L & \text{for} \quad z\le 0 \\ \lim\limits_{z\to-\infty} T=T_e=\text{const} & & \text{for} \quad 0<y<L \\ \lim\limits_{z\to+\infty} T=T_{fd}(y) & & \text{for} \quad 0<y<L \end{cases} \tag{14}$$

Case II: constant wall heat flux

$$\begin{cases} \dfrac{\partial T}{\partial y}=0 & \text{at} \quad y=0 & \text{for} \quad 0<z \\ k\dfrac{\partial T}{\partial y}=q_{\text{lw}} & \text{at} \quad y=L & \text{for} \quad 0<z \\ \dfrac{\partial T}{\partial y}=0 & \text{at} \quad y=0 & \text{for} \quad z\le 0 \\ \dfrac{\partial T}{\partial y}=0 & \text{at} \quad y=L & \text{for} \quad z\le 0 \\ \lim\limits_{z\to-\infty} T=T_e=\text{const} & & \text{for} \quad 0<y<L \\ \lim\limits_{z\to+\infty} T=T_{fd}(y,z) & & \text{for} \quad 0<y<L \end{cases} \tag{15}$$

The bulk temperature and Nusselt number are defined as

$$T_{\text{b}}\equiv\frac{\int_0^L uT dy}{\int_0^L u dy} \tag{16}$$

$$Nu\equiv\frac{hD_{\text{h}}}{k} \tag{17}$$

where the heat transfer coefficients at the walls are

$$h_{\text{uw}}=\frac{q_{\text{uw}}}{T_{\text{uw}}-T_{\text{b}}}, \quad h_{\text{lw}}=\frac{q_{\text{lw}}}{T_{\text{lw}}-T_{\text{b}}} \tag{18}$$

$$q_{\text{uw}}=-k\left.\frac{\partial T}{\partial y}\right|_{y=0}, \quad q_{\text{lw}}=k\left.\frac{\partial T}{\partial y}\right|_{y=L} \tag{19}$$

The following dimensionless quantities are introduced

$$z^*=z/(Pe\cdot D_h) \tag{20}$$

$$Pe=Re_M\cdot Pr_M. \tag{21}$$

The dimensionless temperature and Brinkman number are defined as:

Case I:

$$\theta=\frac{T-T_e}{T_{\text{lw}}-T_e} \tag{22}$$

$$Br_{\mathrm{I}}=\eta\frac{u_m^2}{k(T_{\mathrm{lw}}-T_e)} \tag{23}$$

Case II:

$$\theta=\frac{k(T-T_e)}{q_{\mathrm{lw}}D_h} \tag{24}$$

$$Br_{\mathrm{II}}=\eta\frac{u_m^2}{q_{\mathrm{lw}}D_h}. \tag{25}$$

With the substitution of the above quantities into the dimensional formulations, the dimensionless energy equation and boundary conditions are obtained as

$$u^*\frac{\partial\theta}{\partial z^*}=\frac{\partial^2\theta}{\partial y^{*2}}+\frac{1}{Pe^2}\frac{\partial^2\theta}{\partial z^{*2}}+Br_j\,\eta_a^*\left(\frac{du^*}{dy^*}\right)^2 \tag{26}$$

$$\text{in}\quad 0<y^*<\frac{1}{2}\quad\text{and}\quad -\infty<z^*<\infty\quad(j=\text{I or II})$$

Case I:

$$\begin{cases}\theta=0 & \text{at}\quad y^*=0 \quad \text{for}\quad 0<z^*\\ \theta=1 & \text{at}\quad y^*=\frac{1}{2} \quad \text{for}\quad 0<z^*\\ \theta=0 & \text{at}\quad y^*=0 \quad \text{for}\quad z^*\le 0\\ \theta=0 & \text{at}\quad y^*=\frac{1}{2} \quad \text{for}\quad z^*\le 0\\ \lim\limits_{z^*\to-\infty}\theta=0 & \text{for}\quad 0<y^*<\frac{1}{2}\\ \lim\limits_{z^*\to+\infty}\theta=\theta_{fd}(y^*) & \text{for}\quad 0<y^*<\frac{1}{2}\end{cases} \tag{27}$$

Case II:

$$\begin{cases}\frac{\partial\theta}{\partial y^*}=0 & \text{at}\quad y^*=0 \quad \text{for}\quad 0<z^*\\ \frac{\partial\theta}{\partial y^*}=1 & \text{at}\quad y^*=\frac{1}{2} \quad \text{for}\quad 0<z^*\\ \frac{\partial\theta}{\partial y^*}=0 & \text{at}\quad y^*=0 \quad \text{for}\quad z^*\le 0\\ \frac{\partial\theta}{\partial y^*}=0 & \text{at}\quad y^*=\frac{1}{2} \quad \text{for}\quad z^*\le 0\\ \lim\limits_{z^*\to-\infty}\theta=0 & \text{for}\quad 0<y^*<\frac{1}{2}\\ \lim\limits_{z^*\to+\infty}\theta=\theta_{fd}(y^*,z^*) & \text{for}\quad 0<y^*<\frac{1}{2}\end{cases} \tag{28}$$

The bulk temperature in the dimensionless form is given by

$$\theta_{\mathrm{b}}\equiv 2\int_0^{1/2}u^*\theta dy^* \tag{29}$$

Nusselt numbers at the walls

Case I:

$$Nu_{\mathrm{uw}}=-\frac{1}{(\theta_{\mathrm{uw}}-\theta_{\mathrm{b}})}\left.\frac{\partial\theta}{\partial y^*}\right|_{y^*=0} \tag{30}$$

$$Nu_{\mathrm{lw}}=\frac{1}{(\theta_{\mathrm{lw}}-\theta_{\mathrm{b}})}\left.\frac{\partial\theta}{\partial y^*}\right|_{y^*=1/2} \tag{31}$$

Case II:

$$Nu=\frac{1}{(\theta_{\mathrm{lw}}-\theta_{\mathrm{b}})}. \tag{32}$$

For infinitely large values of the axial distance ($z^*\to\infty$), thermally fully developed region is reached.

For Case I, in the fully developed region the dimensionless temperature is a function of y^* alone. Then the dimensionless temperature θ_{fd} corresponding to the boundary condition of constant wall temperature is the particular solution of the following equation.

Case I:

$$\frac{\partial^2\theta_{fd}}{\partial y^{*2}}=-Br_{\mathrm{I}}\eta_a^*\left(\frac{du^*}{dy^*}\right)^2 \tag{33}$$

$$\begin{cases}\theta_{fd}=0 & \text{at}\quad y^*=0\\ \theta_{fd}=1 & \text{at}\quad y^*=\frac{1}{2}\end{cases} \tag{34}$$

For Case II, since the thermal boundary condition is different from that of Case I, the fully developed temperature profile is calculated in a different fashion. To seek the expression of θ_{fd}, a solution of the following form is assumed taking account of the fact that in the thermally fully developed region, the constant heat flux through the wall will result in a rise of the fluid temperature linearly with the axial coordinate.

Case II:

$$\theta_{fd}=Cz^*+\psi(y^*) \tag{35}$$

Substitution of Eq. (35) into Eq. (26) yields

$$\frac{d^2\psi}{dy^{*2}}=Cu^*-V \tag{36}$$

$$\begin{cases}\frac{d\psi}{dy^*}=0 & \text{at}\quad y^*=0\\ \frac{d\psi}{dy^*}=1 & \text{at}\quad y^*=\frac{1}{2}\end{cases} \tag{37}$$

where

$$V=Br_{\mathrm{II}}\eta_a^*\left(\frac{du^*}{dy^*}\right)^2. \tag{38}$$

On the other hand, in the thermally developed region

$$\rho c_p u\frac{dT_{\mathrm{b}}}{dz}=k\frac{\partial^2T_{fd}}{\partial y^2}+\eta_a\left(\frac{du}{dy}\right)^2 \tag{39}$$

$$\begin{cases}\frac{\partial T_{fd}}{\partial y}=0 & \text{at}\quad y=0\\ \frac{\partial T_{fd}}{\partial y}=q_{\mathrm{lw}} & \text{at}\quad y=L\end{cases} \tag{40}$$

dT_{b}/dz in Eq. (39) is evaluated, from an energy balance, as

$$\frac{dT_{\mathrm{b}}}{dz}=\frac{q_{\mathrm{lw}}}{\rho c_p u_m L}\left[1+\frac{\int_0^L\eta_a\left(\frac{du}{dy}\right)^2dy}{q_{\mathrm{lw}}}\right] \tag{41}$$

Substitution of the above balance into Eq. (39) gives

$$k\frac{\partial^2T_{fd}}{\partial y^2}+\eta_a\left(\frac{du}{dy}\right)^2=\frac{2q_{\mathrm{lw}}u}{u_mD_h}\left[1+\frac{\int_0^L\eta_a\left(\frac{du}{dy}\right)^2dy}{q_{\mathrm{lw}}}\right] \tag{42}$$

By introducing the relevant dimensionless quantities, the above equation becomes

$$\frac{\partial^2\theta_{fd}}{\partial y^{*2}}=2u^*\left(1+\int_0^{0.5}Vdy^*\right)-V. \tag{43}$$

From Eqs. (35) and (43), the coefficient C in Eq. (36) is obtained as

$$C=2\left(1+\int_0^{0.5}Vdy^*\right). \tag{44}$$

$\psi(y^*)$ was calculated from Eq. (36) with Eq. (37) by the finite difference method. The calculation

results of θ_{fd} for Case I and Case II were used as the boundary conditions at downstream infinity.

In order to transform the upstream and downstream infinities into a finite domain, the dimensionless axial coordinate z^* is transformed according to the relation employed by Verhoff and Fisher[4] as follows:

$$z^*=E\tan\pi z_t \quad \text{or} \quad z_t=\frac{1}{\pi}\arctan\frac{z^*}{E}. \qquad (45)$$

By introducing the transformed coordinate z_t, the solution domain along the axial coordinate becomes $-0.5\leq z_t\leq 0.5$. The constant of the axial transformation, E, in Eq.(45) was chosen as 4.62 for Case I and as 1.0 for Case II. An irregular mesh system (100×400) consisting of finer grids near $z_t=0$ was applied to allow more accurate calculation of the fluid axial heat conduction effect. The dimensionless temperature has been numerically solved by the Gauss-Seidel method for the elliptic type of energy equation (26) with the boundary conditions of Eq.(27) or (28) using η_a^*, u^* and du^*/dy^* determined from the fluid flow analysis.

3. Results and Discussion

To check the accuracy of the numerical solutions, our results for the case of a Newtonian fluid ($n=1$) with $Br=0$ (no viscous dissipation) and $Re\to\infty$ (no fluid axial heat conduction) were compared with those presented in Refs.(5) and (6) for $U^*=0$ (stationary walls) and for $U^*=1$ (moving lower wall), respectively. Both solutions on Nusselt number are in excellent agreement with the error of 1%. The predicted results for the case of $n=0.5$ and $\beta=1$ (a pseudoplastic fluid) are discussed hereinafter.

3.1 Temperature development

The temperature distributions of the fluid for $-\infty<z<+\infty$ in parallel plates have been calculated for Case I and Case II.

Case I: Constant wall temperature

Figures 3 and 4 illustrate the variations of local fluid temperature development for the cases of the relative velocity $U^*=0$ and $U^*=1$, respectively. At $z^*=0$, there is a step change in the wall temperature. It is seen that the fluid temperature increases due to fluid axial heat conduction and viscous dissipation before the fluid enters into the heated wall region with finite small Pe and large Br.

In Figs. 3(a) and 4(a) for $Pe\to\infty$ and $Br=0$, at $z^*=0$ ($0<y<L$) the dimensionless temperature of the fluid is zero. But for $Pe=10$ and $Br=0$ in Figs. 3(c) and 4(c) the fluid temperature increases at negative values of z^*. This indicates that the influence of axial heat conduction in the fluid for $z^*\leq 0$ vanishes with increasing Peclet number.

From Figs. 3(b), 3(d), 4(b) and 4(d) for $Br=$

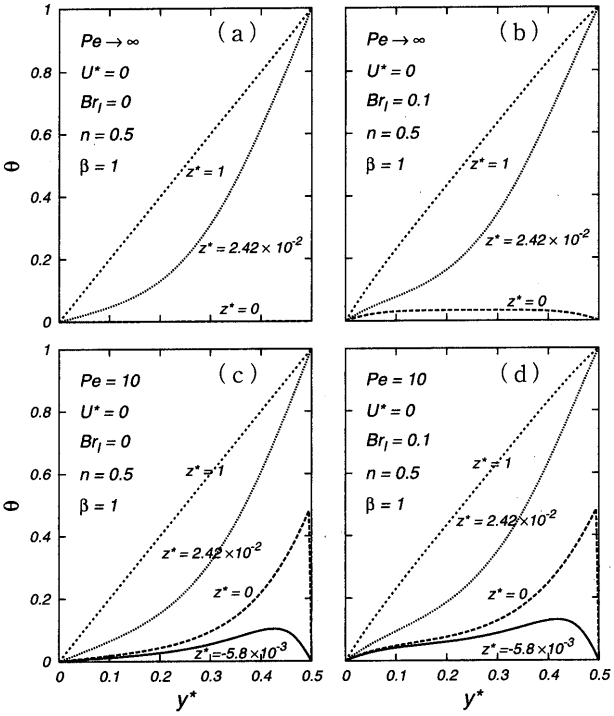

Fig. 3 Developing temperature profiles ($U^*=0$) $n=0.5$, $\beta=1$, Case I

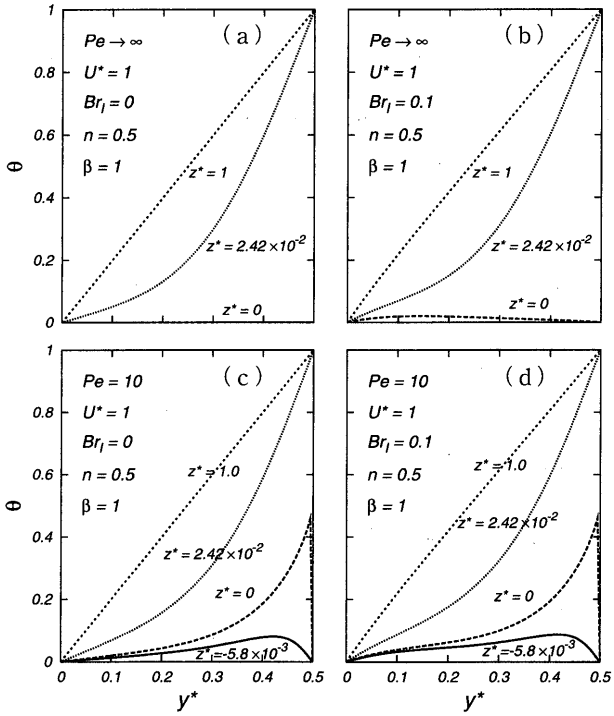

Fig. 4 Developing temperature profiles ($U^*=1$) $n=0.5$, $\beta=1$, Case I

0.1 it can be seen that the dimensionless temperature of the fluid at $z^*<0$ deviates distinctively from zero. This increase is due to the contribution of viscous dissipation in the flowing fluid. Since the highest shear rate occurs near the stationary wall as it is seen in Fig. 2, the effect of viscous dissipation is most

significant near the stationary wall and it is seen from Figs. 3(b) and 4(b) that the temperature increase due to viscous dissipation is greater for $U^*=0$ than for $U^*=1$. Therefore it is observed in Figs. 4(c) and 4(d) that the temperature increase of the fluid due to fluid axial heat conduction and viscous dissipation for the case of moving wall ($U^*=1$) is less than for the case of stationary wall ($U^*=0$).

Case II: Constant wall heat flux

In Fig. 5 the development of temperature profiles is shown for the thermal boundary condition of Case II. The figures on the right-hand show the temperature profiles of the case of the moving lower wall ($U^*=1$). The solid and dashed lines stand for the results for negligible ($Pe\to\infty$) and considerable ($Pe=10$) fluid axial heat conduction cases, respectively. In the region with the insulated walls ($z^*<0$) the fluid temperature is seen sufficiently large for large Br and small Pe. In fact, it can be seen from Figs. 5(c) and 5(d) that the fluid temperature increases significantly before the fluid reaches the heated wall because of the heat generated by viscous dissipation and the heat conducted from downstream into the insulated wall region. The comparison of the temperature profiles for $U^*=0$ and $U^*=1$ shows that the viscous dissipation effect is greater in the case of stationary walls. As this effect builds up, heat is transferred to the main body of the fluid flow and heat generation due to viscous dissipation behaves like a heat source. It is observed that the viscous heating is more pronounced

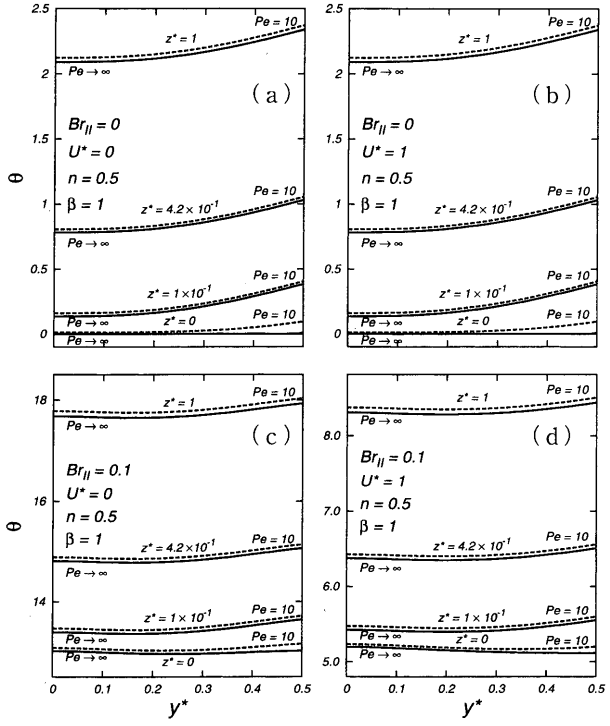

Fig. 5 Developing temperature profiles for $U^*=0$ and $U^*=1$ (Case II)

for the thermal boundary condition of Case II than for that of Case I. The resulting increase in temperature is specially large when the velocity gradient at the fixed wall assumes a large value as it is seen in Fig. 5(c) and Fig. 2. Also from the developing temperature profiles, it is seen for Case II that the wall-to-fluid temperature difference is small.

3.2 Nusselt number

The effects of viscous dissipation, fluid axial heat conduction and moving boundary on Nusselt number are presented in more detail in Figs. 6 to 13.

Case I: Constant wall temperature

The effect of fluid axial heat conduction is demonstrated in Fig. 6 for a Newtonian fluid ($n=1$) with neglected viscous dissipation. The circles show the results from the Refs.(5) and (6) for $Br_1=0$, and even at small values of z^* it is seen that the agreement is excellent. It is also seen that Nusselt number at the upper wall (whose temperature is maintained at a constant value equal to the entering fluid temperature) remains almost constant throughout the thermal entrance region if Pe is small. This behavior is attributed to that the fluid temperature increases due to the fluid axial heat conduction (for $z^*<0$) before the fluid flow reaches the heated wall. It is seen that in the thermally developing region Nusselt numbers at the walls increase due to larger fluid axial heat conduction if viscous dissipation effect is negligible.

The same trend is observed for non-Newtonian fluids. In Figs. 7 and 8, Nusselt number variations in the thermally developing region are shown for a pseudoplastic fluid ($n=0.5$, $\beta=1$) with $Br_1=0$ and $Br_1=0.1$, respectively. It can be observed that the asymptotic Nusselt number values are identical regardless of Pe values. Including fluid axial heat conduction causes an increase in Nusselt number at the lower wall in the thermal entrance region. For a specified axial position with a given Brinkman number, Nusselt number at the lower wall is larger for $U^*=1$ than for $U^*=0$. But Nusselt number at the upper wall whose temperature is kept equal to the entering fluid is larger in the case of $U^*=0$ than in the case of $U^*=1$ for $Br\neq0$. Including viscous dissipation causes an increase in Nusselt number at the upper wall. For $n=0.5$ and $\beta=1$, the fully developed Nusselt number at the upper wall changes from 4.0 to 4.903 for $U^*=0$ and from 3.495 to 4.051 for $U^*=1$ if Br is increased from 0 to 0.1.

The variation of Nusselt number was investigated from the viewpoint of the combined effects of viscous dissipation and fluid axial heat conduction. From Fig. 9 it can be observed that the effect of fluid axial heat conduction ($Pe=10$) accounts for the Nu value increase at the lower wall in the thermal

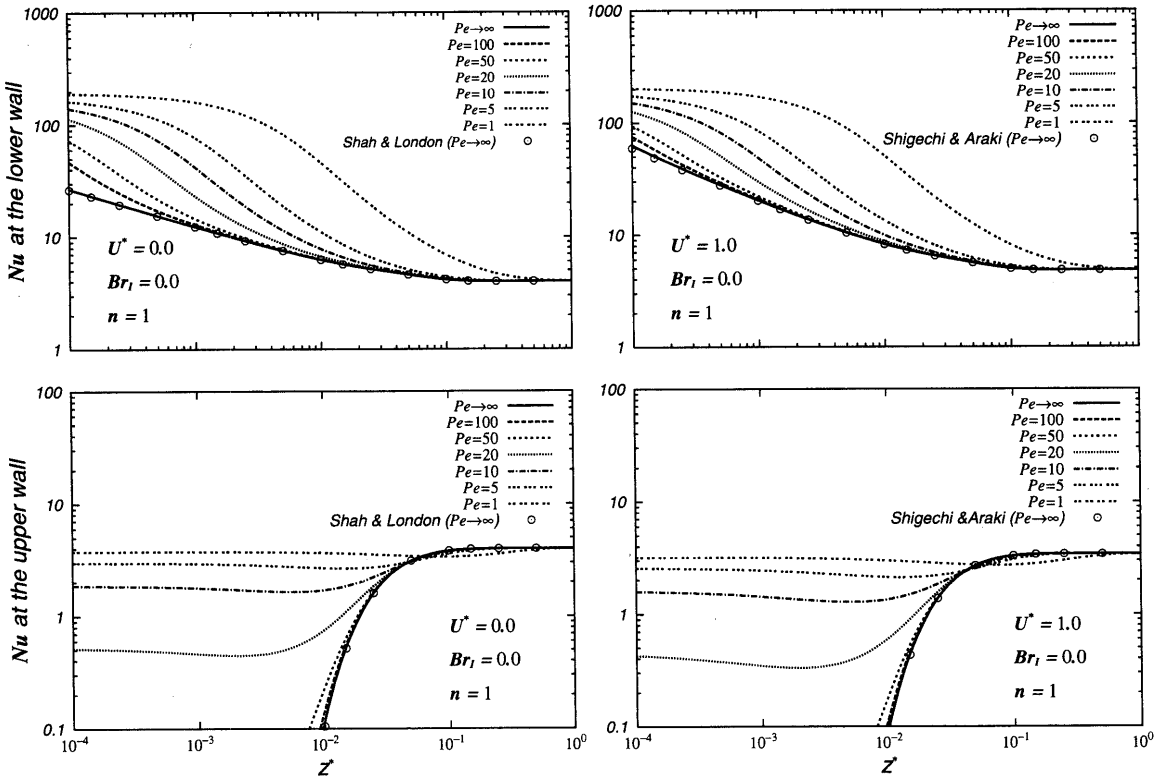

Fig. 6 *Nu* variations with *Pe* for heat transfer to a Newtonian fluid ($n=1$) without viscous dissipation ($Br=0$), Case I

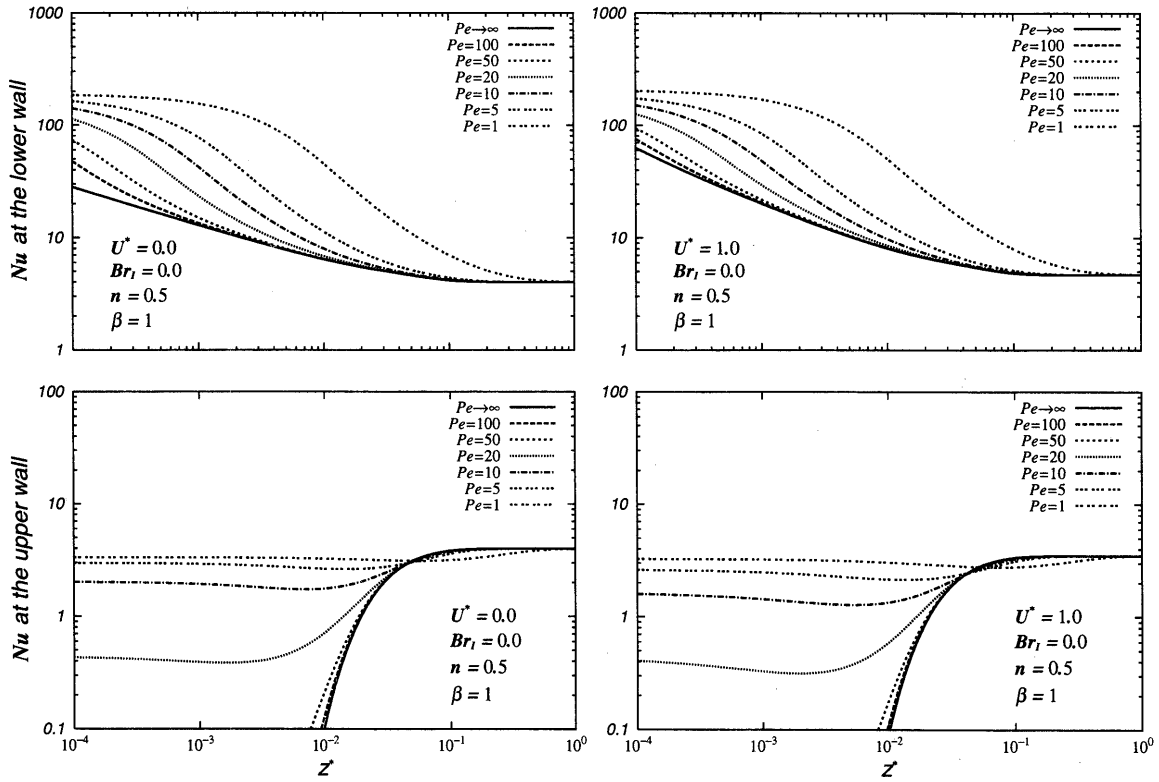

Fig. 7 *Nu* variations with *Pe* for heat transfer to a pseudoplastic fluid ($n=0.5$, $\beta=1$) without viscous dissipation ($Br=0$), Case I

entrance. Viscous dissipation effect ($Br\neq0$) has a strong effect on the Nusselt number at the upper wall. But *Nu* curves at the lower wall are almost identical for different values of *Br* for the same Peclet number if $U^*=1$. For $U^*=0$ Nusselt number at the lower wall decreases with an increase in Brinkman number

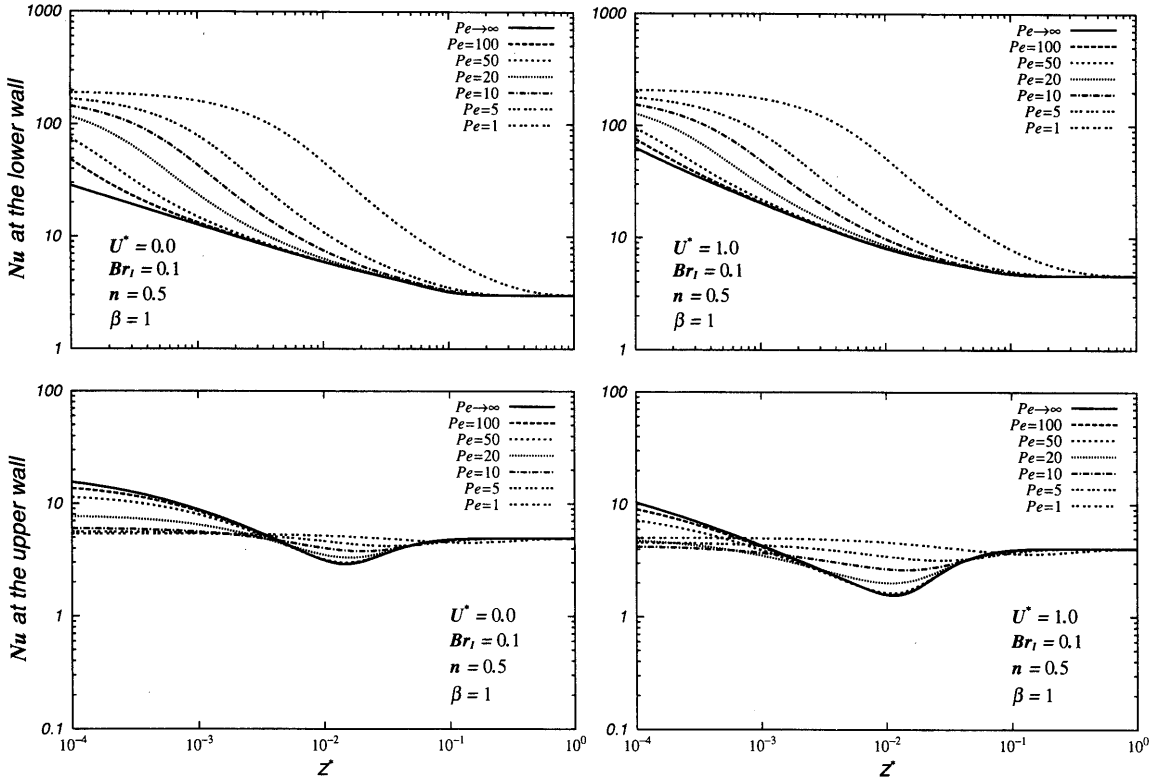

Fig. 8 Nu variations with Pe for heat transfer to a pseudoplastic fluid (n=0.5, β=1) with significant viscous dissipation (Br=0.1), Case I

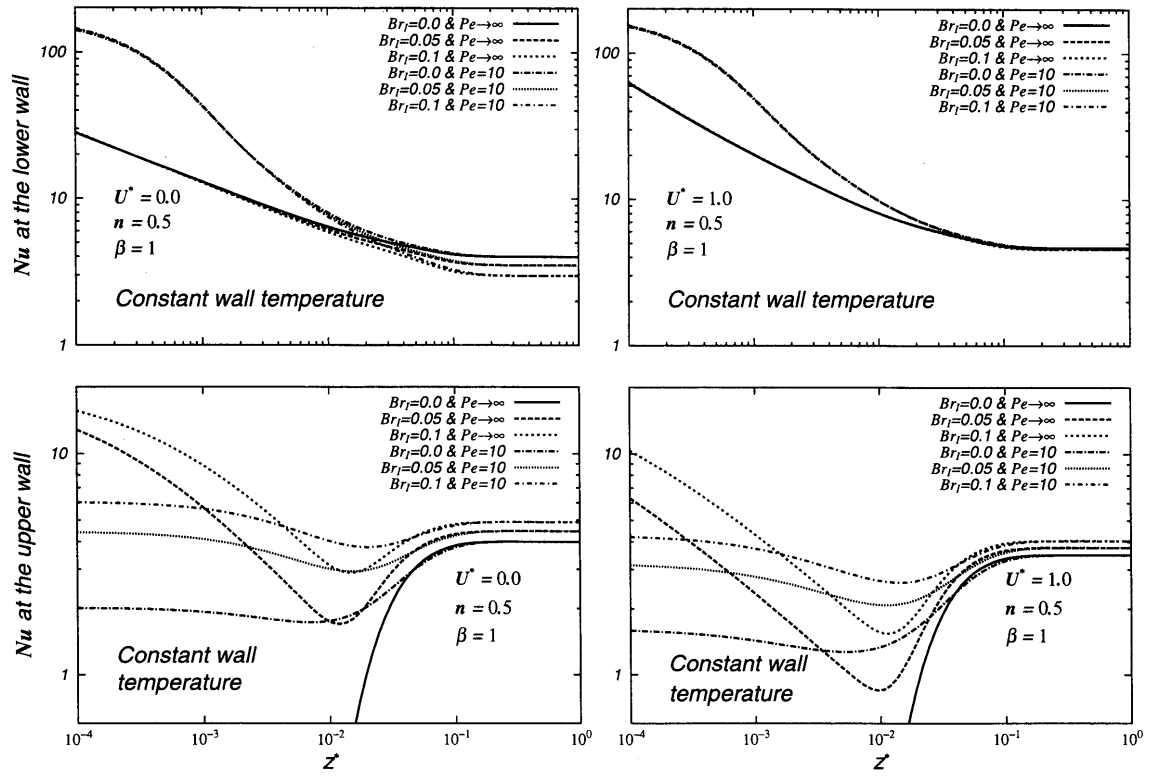

Fig. 9 Effects of Br and Pe on Nu at the walls for Case I (n=0.5, β=1)

in the fully developed region.

Case II : Constant wall heat flux

In Figs. 10 to 13, the variations of Nusselt number are shown with different values of Pe and Br for the thermal boundary condition of Case II. The effect of fluid axial conduction is demonstrated in Fig. 10 for a Newtonian fluid flow with neglected viscous dissipation. The circles show the predictions from the Refs.

(4) and (5). The figures indicate that the agreement of both is excellent. In Figs. 11 and 12 the effect Peclet number on Nusselt number at the heated wall is shown for a pseudoplastic fluid ($n=0.5$, $\beta=1$) with respect to negligible ($Br_{II}=0$) and considerable ($Br_{II}=0.1$) viscous dissipation cases, respectively. Unlike the case of constant wall temperature, Nu values at the heated wall tend to decrease near $z^*=0$ with a decrease in Pe. It is also observed that Nusselt number in the thermal entrance region remains almost constant if Pe is small. This trend has been also seen for Case I.

From Fig. 13 it is seen that the effect of Br on Nusselt number is different depending on the relative velocity, U^*. In the fully developed region, viscous dissipation has a definite effect for both cases of $U^*=0$ and $U^*=1$. Nu decreases with an increase in Br for the stationary wall case ($U^*=0$) and vice versa for the case of the moving wall ($U^*=1$). The behavior of Nu due to viscous dissipation is understood as follows.

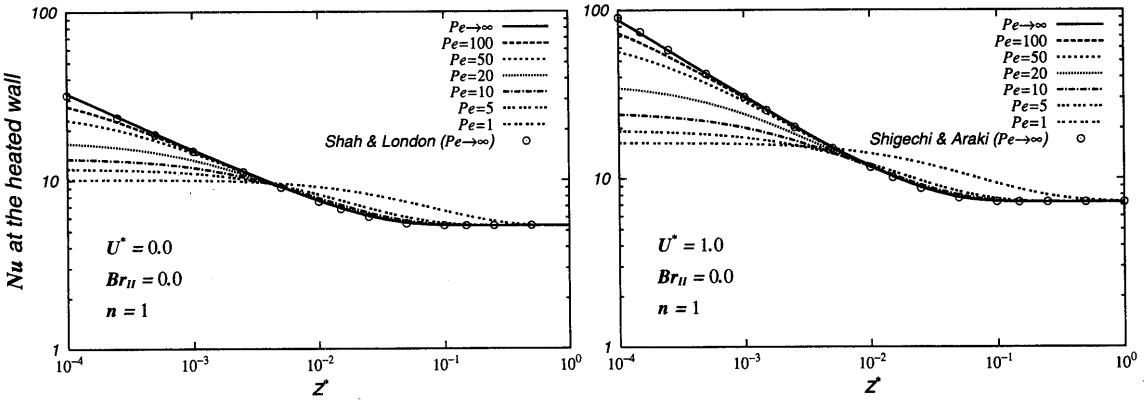

Fig. 10 Nu variations with Pe for heat transfer to a Newtonian fluid ($n=1$) without viscous dissipation ($Br=0$), Case II

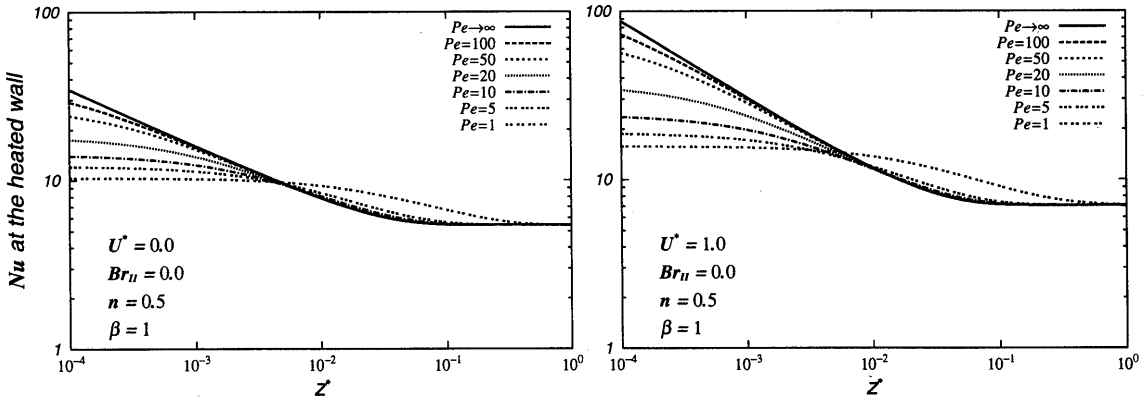

Fig. 11 Nu variations with Pe for heat transfer to a pseudoplastic fluid ($n=0.5$, $\beta=1$) without viscous dissipation ($Br=0$), Case II

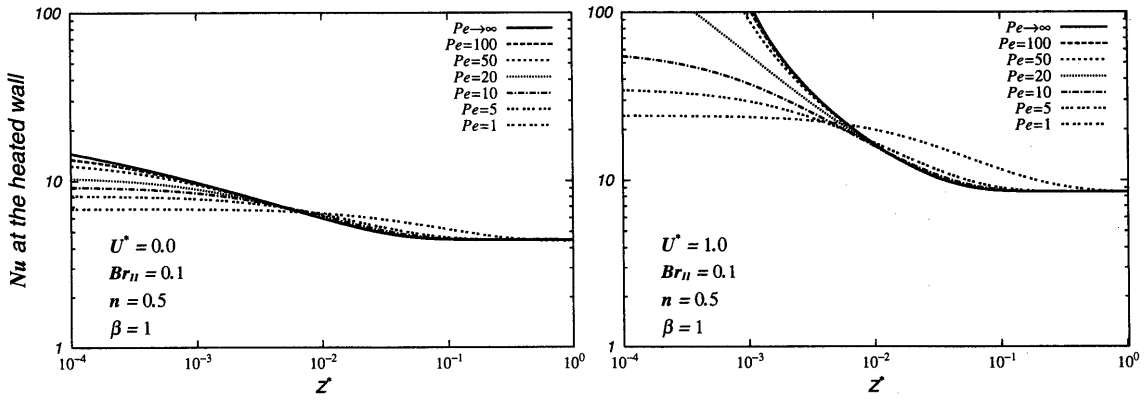

Fig. 12 Nu variations with Pe for heat transfer to a pseudoplastic fluid ($n=0.5$, $\beta=1$) with significant viscous dissipation ($Br=0.1$), Case II

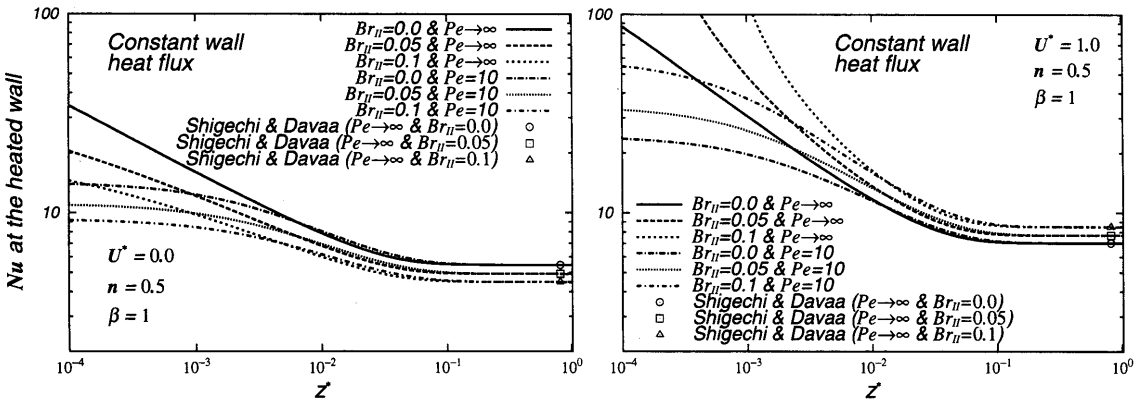

Fig. 13 Fffects of Br and Pe on Nu at the walls for Case II (n=0.5, β=1)

The value of Nu is calculated using the dimensionless temperature difference ($\theta_w-\theta_b$) as shown by Eq.(32). Both of θ_w and θ_b increase in the flow direction of z^*. In terms of the increments of θ_w and θ_b due to viscous dissipation, the increment of θ_w is larger than that of θ_b for $U^*=0$ and vice versa for $U^*=1$.

The effect of fluid axial heat conduction ($Pe=10$) accounts for the decrease in the Nu value in the thermal entrance region.

4. Conclusions

Thermally developing heat transfer of non-Newtonian laminar flow in parallel plates with one plate moving is analyzed including viscous dissipation of the flowing fluid and fluid axial heat conduction for the two kinds of thermal boundary conditions of constant temperature and constant heat flux at the walls as an elliptic type problem by considering an infinite axial domain.

The results are presented graphically in dimensionless form and the effects of the moving plate velocity, fluid axial heat conduction and viscous dissipation are thoroughtly discussed.

An inspection of the temperature profile development reveals that the fluid temperature increases at $z<0$ due to fluid axial heat conduction and viscous heating even when there is no heat flow from the wall. The temperature profiles show a more pronounced effect of viscous dissipation for the case of constant wall heat flux. Nusselt number abruptly decreases for $Pe\to\infty$ and $Br=0$ as the fluid temperature undergoes a rapid change because of the heat flow from the wall. The shape of the Nusselt number curve in the thermal entrance region is rather flattened out for smaller values of Peclet number. This may be explained by the fluid temperature increase in the region of $z<0$. The effect of Br on Nusselt number is different depending on the moving velocity of the plate. For a specified axial position with a given Brinkman number, Nusselt number at the lower wall for $U^*=1$ is larger than the corresponding Nusselt number for $U^*=0$.

For the case of constant wall heat flux, the wall-to-fluid temperature difference is small whereas the effect of viscous dissipation is more significant. Unlike the constant wall temperature case, the Nusselt number at the heated wall is greatly affected by Br in the thermal entrance region for the constant wall heat flux case.

References

(1) Kakac, S., Shah, R.K. and Aung, W., Handbook of Single-Phase Convective Heat Transfer, Chapter 20 (1987), pp. 20.6-20.9, John Wiley & Sons, Inc.

(2) Lin, S.H., Heat Transfer to Plane Non-Newtonian Couette Flow, Int. J. Heat Mass Transfer, Vol. 22 (1979), pp. 1117-1123.

(3) Davaa, G., Shigechi, T., Momoki, S. and Jambal, O., Fluid Flow and Heat Transfer to Modified Power Law Fluids in Plane Couette-Poiseuille Laminar Flow Between Parallel Plates, Reports of the Faculty of Engineering, Vol. 31, No. 57 (2001), pp. 31-39, Nagasaki University.

(4) Verhoff, F.H. and Fisher, D.P., A Numerical Solution of the Graetz Problem With Axial Conduction Included, Trans. ASME, J. Heat Transfer, Vol. 95 (1973), pp. 132-134.

(5) Shah, R.K. and London, A.L., Laminar Flow Forced Convection in Ducts, Advances in Heat Transfer, Suppl. 1, (1978), pp. 284-322, Academic Press.

(6) Shigechi, T., Araki, K. and Lee, Y., Laminar Heat Transfer in the Thermal Entrance Regions of Concentric Annuli With Moving Heated Cores, Trans. ASME, J. Heat Transfer, Vol. 115, No. 4 (1993), pp. 1061-1064; Araki, K., Laminar Heat Transfer in Annuli, Master Thesis, Nagasaki University, (1991).